Remote Sensing of Environment 227 (2019) 125–136

Contents lists available at ScienceDirect

Remote Sensing of Environment

journal homepage: www.elsevier.com/locate/rse

Satellite-based vegetation optical depth as an indicator of drought-driven tree mortality☆

Krishna Rao[a,b,*], William R.L. Anderegg[c], Anna Sala[d], Jordi Martínez-Vilalta[e,f], Alexandra G. Konings[b]

[a] Department of Civil and Environmental Engineering, Stanford University, USA
[b] Department of Earth System Science, Stanford University, USA
[c] School of Biological Sciences, University of Utah, USA
[d] Division of Biological Sciences, University of Montana, USA
[e] CREAF Campus de Bellaterra (UAB), Cerdanyola del Vallès, Spain
[f] Universitat Autònoma Barcelona, Cerdanyola del Vallès, Spain

ARTICLE INFO

Keywords:
Forest mortality
Tree mortality
Vegetation optical depth
Relative water content
Vegetation water content
Climatic water deficit
California drought
AMSR
Random forests

ABSTRACT

Drought-induced tree mortality events are expected to increase in frequency under climate change. However, monitoring and modeling of tree mortality is limited by the high spatial variability in vegetation response to climatic drought stress and lack of physiologically meaningful stress variables that can be monitored at large scales. In this study, we test the hypothesis that relative water content (RWC) estimated by passive microwave remote sensing through vegetation optical depth can be used as an empirical indicator of tree mortality that both integrates variations in plant drought stress and is accessible across large areas. The hypothesis was tested in a recent severe drought in California, USA. The RWC showed a stronger threshold relationship with mortality than climatic water deficit (CWD) – a commonly used mortality indicator – although both relationships were noisy due to the coarse spatial resolution of the data (0.25° or approximately 25 km). In addition, the threshold for RWC was more uniform than that for CWD when compared between Northern and Southern regions of California. A random forests regression (machine learning) with 32 variables describing topography, climate, and vegetation characteristics predicted forest mortality extent i.e. fractional area of mortality (FAM) with satisfactory accuracy-coefficient of determination $R_{test}^2 = 0.66$, root mean square error = 0.023. Importantly, RWC was more than twice as important as any other variable in the model in estimating mortality, confirming its strong link to mortality rates. Moreover, RWC showed a moderate ability to aid in forecasting mortality, with a relative importance of RWC measured one year in advance of mortality similar to that of other relevant explanatory variables measured in the mortality year. The results of this study present a promising new approach to estimate drought stress of forests linked to mortality risk.

1. Introduction

Drought-induced forest mortality events were widespread in recent decades, and were observed on all vegetated continents (Allen et al., 2015). Moreover, climate projections predict added stress – and concomitant mortality – on trees in the future due to rising global temperatures (Williams et al., 2013). Tree mortality can lead to permanent changes in vegetation cover and thus adversely affect ecosystem services such as water quality (Xiong et al., 2011), recreation (McFarlane and Witson, 2008), and timber (Harrison et al., 2014). Furthermore, widespread tree mortality can dramatically escalate fire risk through increases in fire fuels (Hanson and Weltzin, 2000; Bigler and Veblen, 2011; Stephens et al., 2018), and affect water resources through increased stream flow (Bart et al., 2016), and flood risk (Adams et al.,

☆ Authorship: AGK, WRLA, and AS conceived of the study. All authors designed the analyses. KR performed the analyses. KR wrote the first draft of the manuscript, and all authors contributed to interpretation of the data and writing of the manuscript.

Data Accessibility Statement: All authors confirm that if the manuscript is accepted, the data supporting the results will be archived in an appropriate public repository such as GitHub.

* Corresponding author at: 473 Via Ortega, Room 140 Stanford, CA 94305, USA.
E-mail addresses: kkrao@stanford.edu (K. Rao), anderegg@utah.edu (W.R.L. Anderegg), anna.sala@umontana.edu (A. Sala), Jordi.Martinez.Vilalta@uab.cat (J. Martínez-Vilalta), konings@stanford.edu (A.G. Konings).

https://doi.org/10.1016/j.rse.2019.03.026
Received 28 November 2018; Received in revised form 21 February 2019; Accepted 22 March 2019
Available online 13 April 2019
0034-4257/ © 2019 Elsevier Inc. All rights reserved.

2012). Monitoring and forecasting forest mortality occurrence is thus crucial to assess and predict its impacts. While studies of mortality based on observations from forest inventories (Hogg and Kochtubajda, 2005; Malone et al., 2009; Chaparro et al., 2017) are commonplace, inventory measurements are labor-intensive and therefore generally sparse in both time and space. Remote sensing provides a useful alternative.

Most remote sensing studies of mortality have focused on *mapping* tree mortality rather than *modeling* it. Mapping refers to the detection of past mortality by observing land cover related changes (generally using optical reflectance) without relying on any underlying physiological mechanism of mortality, as in the case of modeling. Optical sensors are mainly used for mapping purposes, although some studies do exist that model mortality (see Section 4.2). Past studies have attempted to map tree mortality using change-detection on multispectral imagery from Landsat (Meigs et al., 2011; Meddens et al., 2013), the Moderate Resolution Imaging Spectroradiometer (MODIS; Verbesselt et al., 2009; Byer and Jin, 2017) and other sensors (Tane et al., 2018). There have also been efforts to map mortality using the more advanced hyperspectral imagery (Swatantran et al., 2011; Fassnacht et al., 2014) which gives access to several narrow spectral bands to take advantage of the red-edge property of vegetation (Zarco-Tejada et al., 2002). Such mapping methods can result in high-resolution (≈30 m) mortality maps with low classification error if trained on a small region with uniform vegetation cover. However, mapping mortality using hyperspectral imagery at large scales proves to be a major challenge due to the lack of any publicly-available hyperspectral earth-observing satellites. Furthermore, optical metrics, whether from multispectral or hyperspectral imagery - need to be supplemented with additional data such as high resolution photos (Schwantes et al., 2017) or mortality surveys themselves (Hicke et al., 2016). Such additional data is mainly needed due to the large dependence of optical reflectance on canopy structure and biomass (Tian et al., 2016). Lastly, due to their short wavelengths (≈400 nm to 1300 nm) optical and infrared electromagnetic waves have very limited penetration at the top of the canopy of vegetation and virtually no penetration through clouds. Thus, mapping mortality using multispectral or hyperspectral imagery remains challenging for large scale forest mortality studies.

Alternatively, increased insight could be obtained through *modeling* of mortality and vegetation state, as influenced by its biogeographical conditions and climate. Past approaches to modeling forest mortality (Martínez-Vilalta et al., 2002; McDowell et al., 2008; Anderegg et al., 2015a) – have had limited success. Several studies have tried to predict mortality from empirical climate indicators such as precipitation (Greenwood et al., 2017; Schwalm et al., 2017), temperature (Williams et al., 2013), vapor pressure deficit (Schwantes et al., 2017), climatic water deficit (CWD; Bigler et al., 2007; Van Mantgem and Stephenson, 2007; Anderegg et al., 2015a; Young et al., 2017) and other indicators but such efforts cannot account for the fact that the response of vegetation to drought varies considerably across species. Although plant functional traits can assist in accounting for different responses among (or even within) species (Anderegg et al., 2016), it is almost impossible to model mortality based on them because of the difficulty of parametrizing the species-specific parameters at large spatial scales. Additionally, while some process-based mortality models have seen recent success (Tai et al., 2017), there continues to be significant disagreement between predictions from different models (Mcdowell et al., 2013), likely due to our poor understanding of the complex plant physiology mechanisms leading to mortality (Sala et al., 2010).

In this paper, we argue that passive microwave remote sensing has the potential to be useful for semi-empirical modeling of drought-induced tree mortality because passive microwave observations are directly sensitive to vegetation water content (VWC; Jackson and Schmugge, 1991). The VWC, in turn is closely connected to the relative water content (RWC) – a normalized version of VWC – that directly integrates plant physiological conditions relevant to mortality processes (Kursar et al., 2009; Martinez-Vilalta et al., 2018). A global meta-analysis has previously shown that leaf turgor loss is strongly linked to RWC falling below a threshold, and that this threshold is relatively uniform across species from different biomes (Bartlett et al., 2016). This suggests RWC may be a relatively species-independent indicator of mortality risk (Bartlett et al., 2012). If a similar biome-independent threshold effect can be determined at the canopy-scale and landscape-scale, it may enable semi-empirical mortality modeling based on passive microwave remote sensing of RWC. Such an approach could complement (and overcome some of the shortfalls of) both process-based models (difficulty to parametrize across scales, uncertainty about hydraulic processes) and empirical models that use only climatic indicators.

We tested whether microwave remote sensing-based estimates of RWC can be used to estimate mortality rates at landscape-scale through a case study in California, United States of America. California is home to a wide variety of tree species with a majority of the forested area covered by conifers. The forested region mostly comprises of mixed-conifers, Western Oak and pines. The forests are occasionally threatened by extreme climatic gradients exacerbated by the aggressive fire suppression practices which can result in stand densities as high as 120 per acre (McIntyre et al., 2015). California experienced a severe drought between 2012 and 2016 (Swain et al., 2014), which caused large-scale tree mortality, mostly concentrated in the Sierra Nevada region. The prolonged drought resulted in the death of > 100 million trees since 2010 (USDA, 2016) with pines being the most severely affected (Fig. 1). A key advantage of this study region is that annual tree mortality estimates are available across the entire state, dwarfing the size of most other observational mortality datasets. To evaluate the strength of RWC as a mortality indicator, we initially compared the

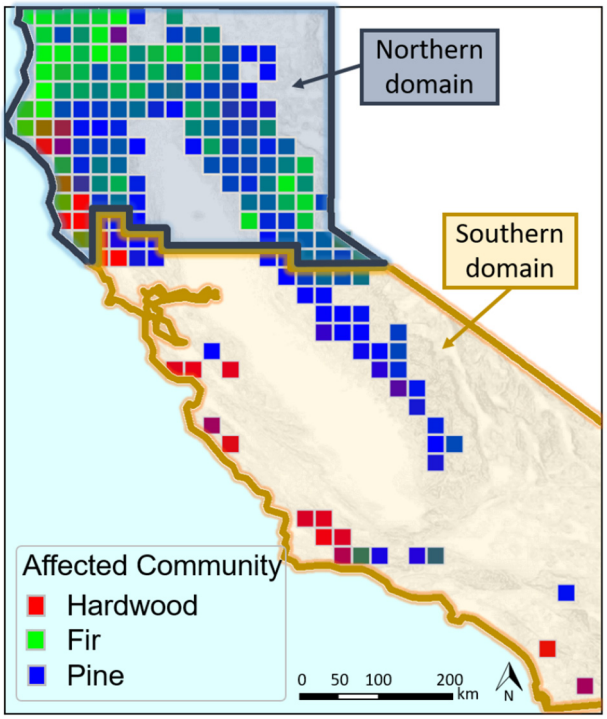

Fig. 1. Map showing the study area and the relative mortality for the affected communities. Each square indicates a 0.25° grid cell (the spatial resolution of this study). The relative strength of individual colors - red, green and blue – compare the mortality extent among the different communities. For example, a pure blue grid cell witnessed only pine mortality. The study area is divided into Northern domain and Southern domains for identifying consistency in mortality thresholds. (For interpretation of the references to color in this figure legend, the reader is referred to the web version of this article.)

direct relationship of each of RWC and CWD to mortality. We then conducted a more in-depth statistical analysis to quantify the unique information available from RWC for mortality modeling. To do so, we used the machine learning algorithm called random forests and built an empirical model with RWC, CWD and alternate input variables related to climate, vegetation, and topography. Our findings demonstrated that RWC performed far better than any other variable as an indicator of tree mortality. Note that while RWC may reflect underlying water stress in trees at the time of mortality or in advance of it, the relationship between RWC and mortality studied here does not directly distinguish whether RWC can be used only for modeling of current mortality or also for forecasting. This difference is further discussed in Section 4.3.

2. Materials and methods

2.1. Datasets used

2.1.1. Tree mortality

The United States Forest Service Pacific Southwest Region has conducted annual surveys of incremental area of dead canopies with the Aerial Detection and Monitoring Program (ADMP; United States Department of Agriculture Forest Service, 2017) since 2005. Since the survey measures incremental area, only the canopy of trees that died in a particular year are recorded in that year. This dataset is one of the most comprehensive mortality datasets in its temporal frequency and spatial extent of revisit; the same region is surveyed every year roughly at the same time of year (July–October). It is based on visual identification of permanent change of tree color to yellow or reddish brown and permanent defoliation. Expert surveyors create annual geotagged sketch maps of incremental canopy area of dead trees based on visual inspection during aerial flights. Background mortality characterized by areas with < 1 tree per acre (4047 m^2) of mortality is generally ignored by the surveyors. The aerial survey spans across most forested regions of California. Because mortality is a slow process that is not perfectly correlated with visible canopy status, and because identification of patches from manual observation is likely to lead to geo-referencing errors, the dataset is imperfect at fine spatial scales. Moreover, the dataset contains mortality majorly due to both droughts and beetle attacks (USDA, 2016) and it can be tricky to isolate the two especially since water-stressed trees are more susceptible to beetle attacks (Anderegg et al., 2015b). Since beetle attacks are also associated with droughts, we refer to both mortality types as drought-driven. Although the survey is not without errors at fine scales and doesn't isolate mortality caused by drought solely, it provides reasonable information about drought-related mortality rates at the resolution and quality required for this study and has been used in other California tree mortality studies (Hicke et al., 2016; Young et al., 2017).

The canopy area of dead trees was re-gridded to 0.25° grid cells to match the spatial resolution of the VOD data used to estimate RWC (see Section 2.1.2). We estimated the severity of mortality extent in each 0.25° grid cell by dividing the canopy area of dead trees by the area of tree cover to obtain the fractional area of mortality (FAM).

$$\mathrm{FAM}_{t,s} = \frac{\text{canopy area of dead trees}_{t,s}}{\text{area of tree cover}_{s}} \quad (1)$$

where t indicates the years from 2009 to 2015, s is a spatial index for each 0.25° grid cell, canopy area of dead trees refers to the incremental area recorded by the ADMP survey, and area of tree cover refers to the time-invariable area of woody cover. This area was determined from the 2009 GlobCover dataset (Arino et al., 2010) which provides high resolution land cover information at 250 m resolution. The study region was chosen as all 0.25° grid cells with > 70% tree cover. The 70% minimum limit for tree cover was selected since the mortality survey was found to be confined to those areas only.

2.1.2. VOD-based relative water content

We used passive microwave remote sensing observations of vegetation optical depth (VOD) to estimate relative water content (RWC). VOD is a dimensionless quantity ranging from 0 to 3. It represents the total attenuation undergone by microwaves due to vegetation which is a result of the sum of the effects of vegetation water and biomass (Jackson and Schmugge, 1991). We used 0.25° resolution X-band VOD from the global Land Parameter Data Record (LPDR; Jones et al., 2011b; Du et al., 2016), version AMSR_E_2_v2. The relatively high frequency of X-Band (10.7 GHz) is not ideal for tree mortality studies since the retrieved VOD is indicative of the water status of leaves and thin branches which only partially reflect the hydraulic health of vegetation. VOD has also been retrieved from L-band sensors such as Soil Moisture Ocean Salinity (SMOS) satellite through the SMOS-IC product (Fernandez-Moran et al., 2017) and the Soil Moisture Active Passive (SMAP; Konings et al., 2017) which are expected to be more sensitive to stem and large branch water content by virtue of their lower frequency and hence deeper penetration. However, L-band-based VOD data have much shorter records as compared to LPDR, so we used LPDR data in this study. The LPDR also has the additional advantage over SMOS-IC that it is not influenced (or at risk of being influenced) by a constant single-scattering albedo selected a priori in its retrieval algorithm (as is the case in the SMOS product). The single-scattering albedo can vary depending on vegetation state (Du et al., 2017) and could thus be variable in both space and time across the study region; an incorrectly parametrized single-scatter albedo value can increase VOD retrieval error.

The LPDR is generated using brightness temperature observations from the Advanced Microwave Scanning Radiometer for Earth Observing System (AMSR-E) and the Advanced Microwave Scanning Radiometer 2 (AMSR-2). The LPDR contains VOD data over all non-precipitating, non-snow, and non-ice terrestrial grid-cells. The LPDR VOD data spans from 2002 to 2015, with a narrow gap from October 2011 to July 2012 between a failure in the AMSR-E sensor and the launch of AMSR-2. The LPDR has been used in several recent studies of vegetation drought response (e.g. Li et al., 2017; Momen et al., 2017) owing to its longer data record at a single frequency.

Although the LPDR uses an inter-calibration of brightness temperatures from AMSR-E and AMSR-2 (Du et al., 2014), it is still possible that a bias exists between the VOD from the two sensors due to imperfections in this inter-calibration that propagate through the VOD retrievals (Du et al., 2017). Indeed, preliminary results suggested such a bias may be present (not shown). We used a cumulative distribution function (cdf) matching technique (Reichle and Koster, 2004) to make the VOD from the two sensors consistent with each other. The bias between AMSR-E and AMSR-2 may be spatially variable, and ideally the cdf-matching would be performed on a local scale. However, because of the stronger drought during the AMSR-2 observational period and the lack of a third overlapping VOD dataset, locally based cdf-matching has the potential to remove a true drought-related signal causing a difference in VOD distributions between AMSR-E and AMSR-2. Instead, the cdf-matching was performed at global scale, consistent with the idea that, when globally averaged across different local climate anomalies, VOD is relatively constant. This assumption is supported by the observation that the global distributions for the periods 2003–2005, 2006–2008, and 2009–2010 were almost identical, with each pair's Kolmogorov–Smirnov statistic < 0.01 and p-value > 0.5 (Fig. S1). Since AMSR-E VOD had a longer timespan (2002 − 2011), it was considered the reference and the cdf of global AMSR-2 VOD (2012–2015) was matched to that of global AMSR-E VOD (2002–2011). For the majority of the pixels, the cdf matching resulted in increased values for AMSR-2 VOD. A sample grid cell with raw AMSR-2 VOD and AMSR-2 VOD after cdf matching is shown in Fig. S2. The final VOD used to estimate RWC was the raw AMSR-E VOD from January 2003–October 2011, and cdf-matched AMSR-2 VOD from August 2012–December 2015.

The VOD has been shown to be directly proportional to vegetation water content (VWC) in field studies of multiple vegetation types (Jackson and Schmugge, 1991), consistent with theoretical expectation (Attema and Ulaby, 1978). The VOD is related to VWC as

$$\mathrm{VOD} = b_s \times \mathrm{VWC} \tag{2}$$

where b is a constant of proportionality dependent on the canopy structure and electromagnetic frequency, and s is a spatial index for each 0.25° grid cell. The b_s depends on the vegetation structure (Van De Griend and Wigneron, 2004) and is therefore assumed constant in time but variable in space. Although the b_s can in theory vary in time with changes in vegetation structure due to mortality, the effect of this change is expected to be relatively small. This assumption is further discussed in Section 4.1. The linearity between VOD and VWC has been well documented for L-band and C-band but not for the 10.7 GHz X-band used in this study (Jackson and O'Neill, 1990). Because of the relatively higher frequency of the AMSR-E signal, it is likely less sensitive to the lower reaches of the canopy. Nevertheless, because this study does not distinguish between differences in RWC across different canopy heights, this effect is neglected. That is, we assume the VOD penetrates a sufficiently large fraction of the canopy that the VWC dynamics are consistent with the whole-tree VWC dynamics.

The VWC at any time depends on both the above-ground biomass and RWC of trees. At 0.25° resolution, it is unlikely that all the vegetation cover in a grid cell is ever dried out completely or completely saturated. We therefore calculated RWC by using a location-dependent normalization for VOD. We assumed that the lowest and highest VWC observed for each grid cell during a sufficiently long period (2003–2015) corresponded to the typical dry state and typical wet state of the trees, respectively. To reduce the effect of high-frequency noise inherent in most VOD datasets (Konings et al., 2015, 2016), rather than using the lowest and highest values of VOD we used 5th percentile and 95th percentile, respectively. In each year, the RWC was calculated as the median value over the summers only (1st July to 30th September); the season with the greatest drought stress. The interannual variations in RWC were qualitatively insensitive to the exact choice of summer season. We then extended the conceptual definition of RWC from a single tissue or tree to all trees in each grid cell:

$$\mathrm{RWC}_{t,s} = \frac{\mathrm{median}_{t,s}(\mathrm{VWC}) - 5^{\mathrm{th}}\mathrm{percentile}_s(\mathrm{VWC})}{95^{\mathrm{th}}\mathrm{percentile}_s(\mathrm{VWC}) - 5^{\mathrm{th}}\mathrm{percentile}_s(\mathrm{VWC})} \tag{3}$$

where t indicates the summer of each year and s refers to the index of 0.25° grid cells. Because b_s is assumed to be time-independent, RWC is estimated directly from VOD by multiplying the numerator and denominator of Eq. (3) by b_s:

$$\mathrm{RWC}_{t,s} = \frac{\mathrm{median}_{t,s}(\mathrm{VOD}) - 5^{\mathrm{th}}\mathrm{percentile}_s(\mathrm{VOD})}{95^{\mathrm{th}}\mathrm{percentile}_s(\mathrm{VOD}) - 5^{\mathrm{th}}\mathrm{percentile}_s(\mathrm{VOD})} \tag{4}$$

We used ascending pass observations from AMSR-E and AMSR-2 with local overpass time of 1:30 pm since this is close to the time of day of greatest drought stress. Fig. 2 illustrates the derivation of RWC for a sample grid cell. Further information on canopy greenness status and atmospheric conditions for the same grid cell is provided in Fig. S3 by showing leaf area index and maximum vapor pressure deficit.

2.1.3. Climatic water deficit

Among the many different climate-based predictors used in empirical models of mortality, climatic water deficit (CWD) has been the most common (e.g. Bigler et al., 2007; Van Mantgem and Stephenson, 2007; Anderegg et al., 2015a; Young et al., 2017). The CWD is the difference between potential evapotranspiration and actual evapotranspiration (Stephenson, 1998). Since CWD represents the amount by which evapotranspiration is suppressed (for example through stomatal closure) relative to conditions under which water is not limiting, it can reflect the water stress on vegetation, but only indirectly. The CWD

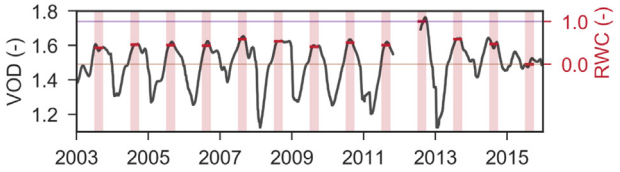

Fig. 2. Derivation of RWC for a sample grid cell. Solid line represents 30-day smoothed VOD. VOD data smoothed for illustrative purposes only. Shaded vertical red band denotes summer period between 1-July to 30-Sep. The brown line indicates 5th percentile and the purple line indicates 95th percentile VOD over all summers. Dark red horizontal lines in each summer represent RWC level for the respective year (from the brown line). The (−) symbol indicates unit-less quantities. The FAM for the grid-cell in year 2015 was 0.05. (For interpretation of the references to color in this figure legend, the reader is referred to the web version of this article.)

estimates by Young et al. (2017) were used in our study. The components of CWD – potential evapotranspiration and actual evapotranspiration – were derived in this dataset using a modified Thornthwaite approach (Willmott et al., 1985) with precipitation data from the Parameter-elevation Regression on Independent Slopes Model (PRISM) Climate Group (PRISM Climate Group Oregon State University, 2016) and temperature data from the TopoWx data set (Oyler et al., 2015). The resulting CWD was accumulated for every water year from 2009 to 2015 by Young et al., with each water year spanning from October of the preceding year to September of the current year.

2.1.4. Alternate input variables

We used a machine learning model to estimate and forecast tree mortality with multiple inputs to test the hypothesis that RWC is the strongest indicator of tree mortality in the presence of other widely used mortality input variables. As many variables that could potentially affect drought-driven mortality rates and were available across the study area for the required period were included.

Topographic variables such as time-invariant mean and standard deviation of elevation along with mean and standard deviation of aspect (found to be significant predictors by Worrall et al., 2008; Tai et al., 2017) were included. Aspect and elevation data were obtained from National GAP Analysis Project (USGS, 2011b) and National Elevation Dataset (USGS, 2011a), respectively. Additionally, mean and standard deviation of topographic wetness index (TWI; Beven et al., 1979) which is a function of local topography and slope was included since TWI was found to be a significant predictor of mortality by Kaiser et al. (2013). The TWI is defined as $\log_e\left(\frac{a_c}{\tan(b)}\right)$, where a_c is the upslope contributing area of water flow along hill-slopes per unit contour length and $\tan(b)$ is the local land surface slope. It was obtained from the HYDRO1k data set (USGS, 2000) developed using the Global 30 Arc-Second Elevation (GTOPO30) digital elevation model. Along with topographic variables, geographic variables such as soil properties were also included as they may influence spatial patterns of mortality (De Toledo et al., 2011). The top soil sand fraction and silt fraction (obtained from Liu et al., 2014) were used as two separate inputs. The clay fraction was ignored as it is equal to 1 − (sand fraction + silt fraction). Consistent with standard practice for the use of machine learning in environmental studies, we also included location information after converting each pair of latitude and longitude of grid cells into a factor variable. The location input partially accounted for spatial auto-correlations in mortality, if any existed.

Variables related to vegetation included fraction of forest cover (from Arino et al., 2010), canopy height (obtained from Geoscience Laser Altimeter System; Simard et al., 2011), live basal area (obtained from the Graph Neural Network Dataset; Land Ecology Modeling and Analysis Group, 2015), leaf area index (LAI) and Normalized Difference Water index (NDWI). Canopy height and live basal area were used because previous studies have shown competition among trees to be

correlated with mortality (Young et al., 2017). Due to lack of time-variable observations, canopy height was assumed to be constant during the study period. Annual estimates of live basal area were obtained from Young et al. (2017). Reprocessed LAI from the MODIS Terra product MOD15A2 (Yuan et al., 2011) was used as an indicator of biomass reductions during drought (Bréda et al., 2006). The reprocessed LAI dataset uses quality control information along with a spatio-temporal filter to produce more accurate and continuous maps than the original dataset. The NDWI – a widely used shortwave infrared-based drought stress metric (Gu et al., 2007; Byer and Jin, 2017) was included to provide a direct comparison to its microwave counterpart (RWC). The NDWI was calculated from the MODIS Terra and Aqua nadir-adjusted reflectance product MCD43A4.V006 (Schaaf and Wang, 2015) using the definition $NDWI = (\rho_{0.86\mu m} - \rho_{1.24\mu m})/(\rho_{0.86\mu m} + \rho_{1.24\mu m})$ from Gao (1996) where ρ refers to the reflectance values.

Climate related variables such as potential evapotranspiration and actual evapotranspiration (constituents of CWD), maximum vapor pressure deficit, mean and maximum temperature (shown to affect mortality in *Pinus edulis* by Adams et al., 2013; and in conifer species by Williams et al., 2013), precipitation, and surface soil moisture were included. Potential evapotranspiration and actual evapotranspiration were obtained from the Noah land surface model in the North American Land Data Assimilation System (NLDAS; Xia et al., 2012). Precipitation, temperature, and maximum vapor pressure deficit were obtained from PRISM and surface soil moisture was obtained from the LPDR. While it is possible that the LPDR may misdiagnose part of the soil moisture signal to the VOD output or vice-versa, we expect such errors to be on the low end because the LPDR algorithm uses both horizontal and vertical polarization brightness temperatures to distinguish between the two. All climatic variables except CWD – for which monthly data was not available – were split by season into summer (July 1st to September 30th) and winter (January 1st to March 31st). All variables were spatially aggregated to a common 0.25° resolution to match the VOD resolution. Table 1 summarizes all variables used.

2.2. Statistical analysis

2.2.1. Breakpoint threshold

Identifying quantitative thresholds in the relationship between a given mortality indicator or risk factor and probability of mortality is a useful step forward towards the modeling and prediction of forest mortality (Hartmann et al., 2018). Anderegg et al. (2015a), for instance, found that above a certain CWD threshold, mortality rates of *Populus tremuloides* in the southwestern United States increased strongly and suddenly. In the case of RWC too, a threshold behavior with FAM is desirable. As argued in Martinez-Vilalta et al. (2018), a mortality risk indicator will ideally fluctuate over a wide range of values above a critical threshold when the vegetation is healthy or when under mild hydraulic stress. It will further show a threshold-like relationship under extreme drought stress corresponding to the rapid decline of water status prior to mortality. We therefore tested whether thresholds existed for either remotely sensed RWC or CWD in estimating FAM. A breakpoint regression analysis was used, wherein two linear least-squares regressions were performed and constrained to be continuous at the break-point value between them. We further tested whether the RWC and CWD are scalable mortality indicators by checking if the respective thresholds varied with vegetation cover. Having a consistent threshold can be advantageous for large scale mortality studies since no in situ information of the threatened tree communities would be required to parametrize the relationship between mortality and the stress indicator. The sensitivity of the RWC (and CWD)-mortality links to vegetation cover was tested by splitting the study area into two regions with different average species coverage – a Northern domain and a Southern domain. We used the survey ID of sub-regions from the ADMP mortality survey to classify 8 northern sub-regions as the Northern domain and 9

Table 1
Details of variables used in the base model. "Season" column refers to period of the year. Summer is defined as July 1st to September 30th, and winter as 1st January to 31st March. The "Time Dependence" column indicates whether each variable was assumed to be constant for the entire study period or not.

Category	Variable Name	Description	Season	Time dependence
Vegetation	Canopy height	Height of canopy	All-year	Constant
	Forest cover	Fraction of woody cover	All-year	Constant
	LAI_{sum}	Leaf area index	Summer	Variable
	LAI_{win}	Leaf area index	Winter	Variable
	$NDWI_{sum}$	Normalized Difference Water Index	Summer	Variable
	$NDWI_{win}$	Normalized Difference Water Index	Winter	Variable
	RWC	Relative water content	Summer	Variable
	Tree density	Basal area of live trees per unit area	All-year	Variable
Topography	Aspect	Mean aspect	All-year	Constant
	$Aspect_{sd}$	Standard deviation of aspect	All-year	Constant
	Elevation	Mean altitude	All-year	Constant
	$Elevation_{sd}$	Standard deviation of altitude	All-year	Constant
	Location	Factored Latitude-Longitude of pixel center	All-year	Constant
	Sand	Mean sand fraction of top-soil	All-year	Constant
	Silt	Mean silt fraction of top-soil	All-year	Constant
	TWI	Mean topographic wetness index	All-year	Constant
	TWI_{sd}	Standard deviation of topographic wetness index	All-year	Constant
Climate	AET_{sum}	Actual evapotranspiration	Summer	Variable
	AET_{win}	Actual evapotranspiration	Winter	Variable
	CWD	Annually accumulated climatic water deficit	All-year	Variable
	PET_{sum}	Potential evapotranspiration	Summer	Variable
	PET_{win}	Potential evapotranspiration	Winter	Variable
	P_{sum}	Precipitation	Summer	Variable
	P_{win}	Precipitation	Winter	Variable
	SM_{sum}	Soil moisture	Summer	Variable
	SM_{win}	Soil moisture	Winter	Variable
	$T_{max,\ sum}$	Maximum temperature	Summer	Variable
	$T_{max,\ win}$	Maximum temperature	Winter	Variable
	T_{sum}	Mean temperature	Summer	Variable
	T_{win}	Mean temperature	Winter	Variable
	$VPD_{max,\ sum}$	Maximum vapor pressure deficit	Summer	Variable
	$VPD_{max,\ win}$	Maximum vapor pressure deficit	Winter	Variable

southern sub-regions as the Southern domain. The Southern domain was both warmer and dryer with mean temperature of 13.4 °C and annual precipitation of 770 mm as compared to the Northern domain which had a mean annual temperature of 11.4 °C and precipitation of 1270 mm during the study period (PRISM Climate Group Oregon State University, 2016). The study area was split for the breakpoint threshold analysis only. The regions are illustrated in Fig. 1. The split was chosen such that both regions had a sufficient number of high mortality pixels, allowing identification of thresholds in each. The break-point thresholds in each of the domains were then compared.

2.2.2. Random forest model

To determine the unique information that RWC can add to tree mortality models, we built a machine learning model based on random forests regression (Breiman, 2001) and ranked the 32 input variables (Table 1) based on their relative importance. The goal of this experiment was not to build the best possible model for operational use, but merely to test whether RWC can provide information about mortality not contained in alternate observations of climate, vegetation and topography conditions. By using a machine learning approach, we were able to test the information content of RWC without assuming an explicit functional form relationship between FAM and RWC.

The random forest model was used because it allows straightforward computation of relative importance of variables towards the predictions. Furthermore, random forests are relatively insensitive to extra inputs that carry little information, allowing us to include many alternate input variables without risking degradation in the model's performance or its ability to identify the most important inputs (Breiman, 2001). Data from 2009 to 2015 were used. This period was limited by the availability of CWD data 2009 onwards and VOD data until 2015. We shuffled pixel-years (grid cell value per unique year) in space and time before splitting them into a training set and a test set in the ratio 70:30, as is standard for medium size datasets. This resulted in a training set size of 835 pixel-years and a test set size of 358 pixel-years. Consistent with standard practice, the random forest trees were fit on the training set to maximize variance explained in observed FAM. During the fitting process, 200 trees were grown, after which the test error stabilized. To prevent overfitting, a maximum of 5 variables were split at each node and nodes with < 8 pixel-years (1% of training set) were disallowed. Finally, to assist the random forest algorithm in optimal training, the probability of each variable being selected for splitting was set inversely proportional to the mean absolute cross-correlation with all other variables. This resulted in more cross-correlated variables being chosen less frequently at the nodes, maximizing the amount of independent information used.

The performance of the model was measured using coefficient of determination (R_{test}^2), root mean square error (RMSE), and mean bias error (MBE). The three metrics are defined below.

$$R_{test}^2 = 1 - \frac{\sum_{i=1}^{m} (y_i - \hat{y}_i)^2}{\sum_{i=1}^{m} (y_i - \bar{y})^2} \quad (5)$$

$$RMSE = \sqrt{\frac{\sum_{i=1}^{m} (y_i - \hat{y}_i)^2}{m}} \quad (6)$$

$$MBE = \frac{1}{m} \sum_{i=1}^{m} (y_i - \hat{y}_i) \quad (7)$$

where, y_i is the observed FAM and $\hat{y}_i$ is the modeled FAM of the ith pixel-year in the test set, $\bar{y}$ is the mean FAM of the test set, and m is the size of the test set. The performance statistics reported in the rest of the paper refer to the model trained on 70% of the data.

The relative importance of the input variables towards the output prediction was computed using the percentage variance explained in the out-of-bag (i.e. cross-validation) data of the training set (1/3rd of the pixel-years in the training set) by each individual variable. Note that the splitting probabilities that were adjusted according to cross-correlations were all reset to 1.0 before computing relative importance of variables so that the importance was not artificially influenced. To estimate the sensitivity of the relative importance to the choice of training set, we varied the fraction of pixel-years used for training from 0.3 to 0.8 in steps of 0.1. We also varied the method of sorting the pixel-years between complete random sampling and a stratified random sampling such that each set had a proportional amount of high mortality pixel-years, and finally varied the random seed initializer to produce a total of 960 model runs. For all random forest results, the mean of the 960 model runs is shown, and the ensemble of 960 model runs is used to generate uncertainty estimates.

In total, three separate random forest models were generated. The first model (hereafter called the base model) was trained on variables from Table 1. Because cross-correlations among input variables can sometimes distort the relative importance of variables, a second model (hereafter called the trimmed model) was run on a reduced set of variables to gain improved confidence of variable importance. This reduced set of variables was selected such that the absolute correlation coefficient between any two variables did not exceed 0.5. Finally, a third model (hereafter called the lagged model) was trained on all variables from Table 1 with the addition of two more variables "$RWC_{1\ year\ lag}$" and "$RWC_{2\ years\ lag}$". They were derived using Eq. (4) but using VOD time series only until the lagged year. This was done to assess the forecasting strength of RWC at yearly timescales. To ensure correct interpretation of the lagged model's variable importance, we checked the correlation between incremental FAM (referred to as just "FAM" earlier) and accumulated FAM. A low correlation was found between FAM and cumulatively-summed FAM ($R^2 = 0.28$ for pixels with FAM ≥ 0.1 and $R^2 = 0.35$ for all pixels, Fig. S4). The implications of this are further discussed in Section 4.1.

Data processing and spatial re-gridding were performed in Python v. 2.7.8 using the ArcPy package. Breakpoint regression was also performed in Python using Scipy (Jones et al., 2011a) while random forests regression was performed in R v. 3.2.2 (R Core Team, 2016) using the Ranger package (Wright and Ziegler, 2015).

3. Results

Fig. 3 shows the break-point regression between FAM and each of RWC and CWD. As expected, pixel-years of lower RWC were often associated with higher FAM (Fig. 3a), though there was considerable scatter in the relationship (combined $R^2 = 0.07$). Even at near-zero RWC values, the mortality rates estimated by the two-step breakpoint regression were well below the highest observed FAM, because there were a lot of near-zero mortality pixel-years at low RWC. Similarly, many high FAM pixel-years occurred for relatively high CWD values (combined regression $R^2 = 0.02$, Fig. 3b), though mortality rates seemed to decrease for the very highest CWD values (e.g. above about 950 mm). The break-point analysis for overall mortality identified an RWC threshold of 0.06 ± 0.01 and a CWD threshold of 594 ± 140 mm. Compared to the dynamic range of the variables, the uncertainty in CWD threshold (140 mm or 14%) dwarfed the uncertainty in RWC threshold (0.01 or 1%), consistent with the stronger relationship between RWC and FAM. Nevertheless, by themselves, neither of the variables was enough to model mortality accurately.

When the break-point regression was separated by region, the RWC thresholds for Northern domain (RWC = 0.05 ± 0.01, Fig. 3c) and Southern domain (RWC = 0.16 ± 0.05, Fig. 3e) differed slightly. However, CWD thresholds differed much more between the Northern (CWD = 637 ± 91 mm, Fig. 3d) and Southern domains (CWD = 1049 ± 40 mm, Fig. 3f), and could not be explicitly compared since the CWD breakpoint regression in the Southern domain showed counter-intuitive results, with a negative relationship between FAM and CWD at high CWD.

None of the alternate input variables individually correlated well

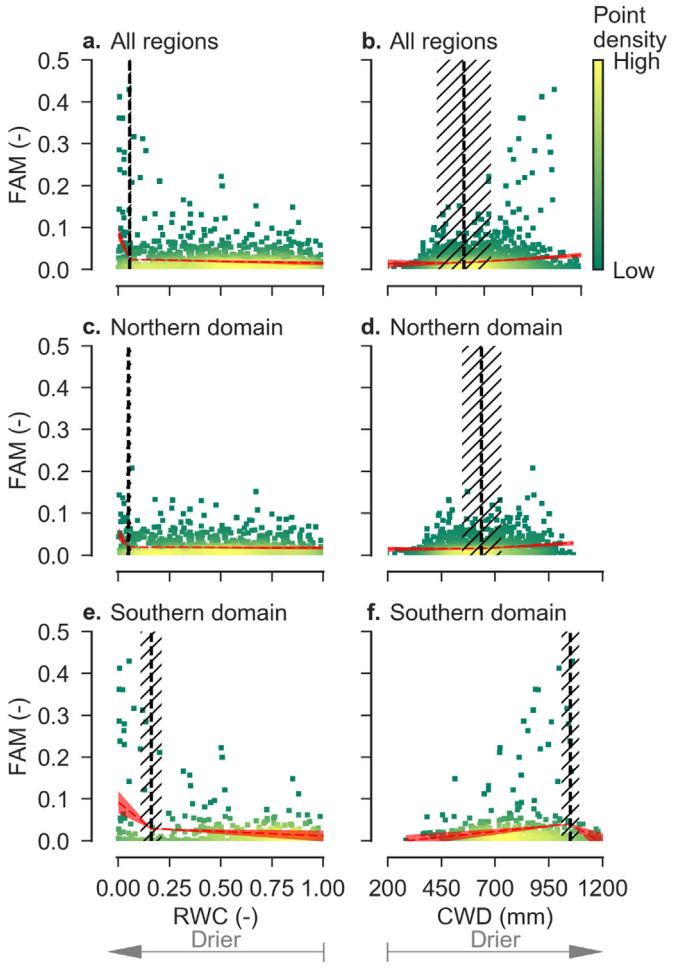

Fig. 3. FAM vs. RWC and CWD. Data presented for all regions in panels (a) and (b), Northern domain in panels (c) and (d), Southern domain in panels (e) and (f). Each point represents a 0.25° grid cell for a unique year. Dashed red lines indicate break-point regression best-fit with shading for ± 1 standard error. Dashed black lines indicate RWC and CWD thresholds with shading for ± 1 standard error. Combined R^2 and threshold values for RWC for (a) all regions = 0.07; 0.06 ± 0.01, (c) Northern domain = 0.03; 0.05 ± 0.01, and (e) Southern domain = 0.12; 0.16 ± 0.05. Combined R^2 and threshold values for CWD for (b) all regions = 0.02; 594 ± 140 mm, (d) Northern domain = 0.02; 637 ± 91 mm, and (f) Southern domain = 0.03; 1049 ± 40 mm (threshold of opposite sign). Points are colored based on their density. The (−) symbol indicates unit-less quantities. (For interpretation of the references to color in this figure legend, the reader is referred to the web version of this article.)

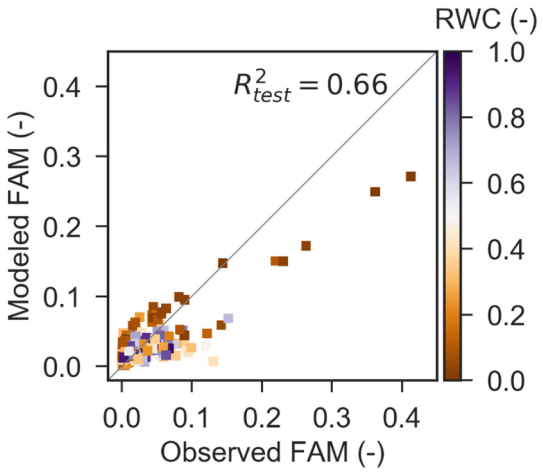

Fig. 5. Base model's performance on test set. Each point is a 0.25° grid cell for a unique year. Points are colored based on relative water content (RWC). The 1:1 line is represented in grey. The (−) symbol indicates unit-less quantities.

with FAM (Fig. S5), rendering a multi-variate method such as random forests the only approach for meaningful modeling of mortality (and interpretation of variable importance). The FAM estimated by the base model correlated well with observed FAM spatially in both high-mortality and low-mortality years (Fig. 4).

When 70% of the data was used for training with stratified random sampling, the base model's performance on the test set was R_{test}^2 = 0.66, RMSE = 0.023, and MBE = −0.001 (Fig. 5). The model's accuracy is much higher than that of previous climate-based empirical models at regional scale (e.g. R^2 = 0.14; Young et al., 2017) and similar to models which had access to physiological field measurements (R^2 = 0.62; Tai et al., 2017). Moreover, RWC showed a consistent relationship with observed FAM, with higher mortality pixel-years commonly having lower RWC (color of points, Fig. 5). Overall, the quality of the base model was sufficient to allow interpretation of the relative importance of its input variables.

The base model identified RWC as the largest contributor towards modeling mortality, with a mean relative importance of 0.11 out of 1.00 (Fig. 6), more than twice as much as the second-largest contributor, elevation (importance = 0.05). By contrast, CWD was only the 7th most important variable at this regional scale (importance = 0.05). It is notable that the random forest model indicated relatively large contributions from elevation (with mean elevation the 2nd most important predictor, importance = 0.05, and standard deviation of elevation the 6th most important predictor, importance = 0.05), which is consistent with both previous mortality modeling (Tai et al., 2017) and mortality estimation (Byer and Jin, 2017) efforts. Across 960 runs of the base model, RWC ranked first in importance in 98.5% of the cases.

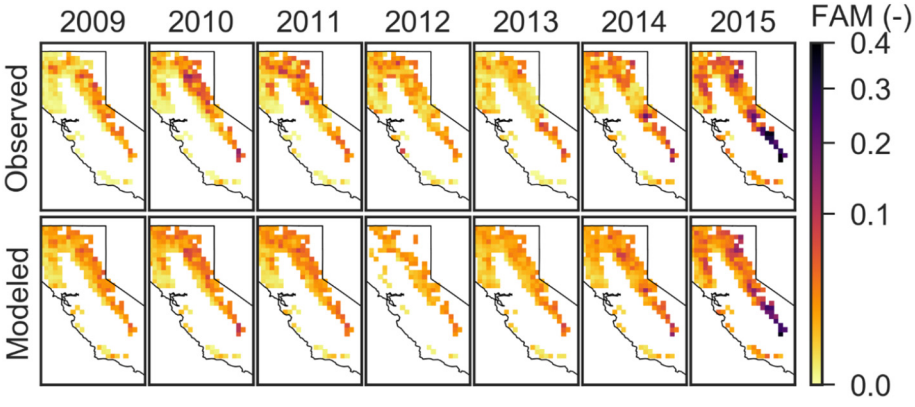

Fig. 4. Observed and modeled FAM from the base model across California. Observed mortality re-gridded to 0.25° to match with resolution of VOD, which had the lowest resolution among all variables. Only grid cells with at-least 70% forest cover were included, and pixels from both the train and test sets are shown in the "Modeled" panel. The (−) symbol indicates unit-less quantities.

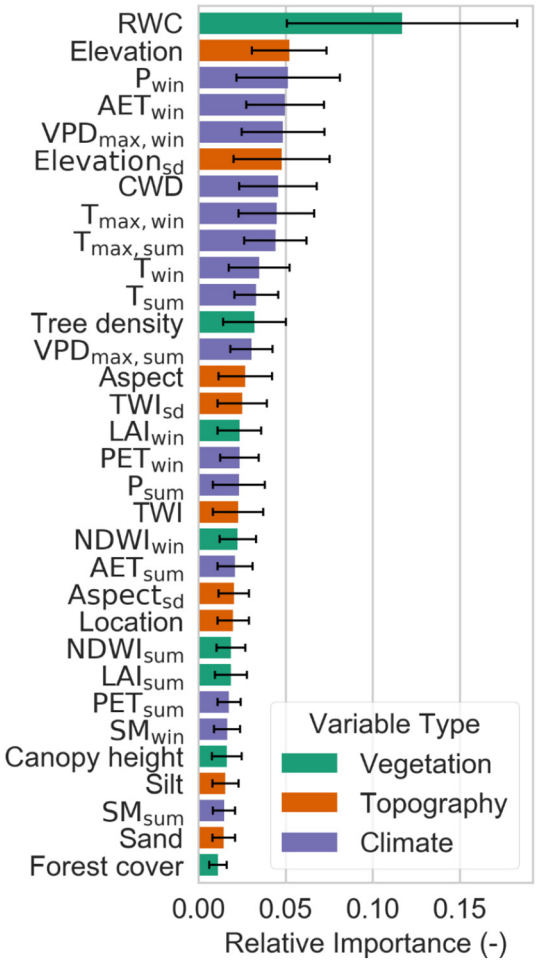

Fig. 6. Relative importance of variables in the base model. Length of bars represent mean relative importance of variables from all 960 model runs. Error bars indicate one standard deviation on each side of mean. Abbreviations as in Table 1. The (−) symbol indicates unit-less quantities.

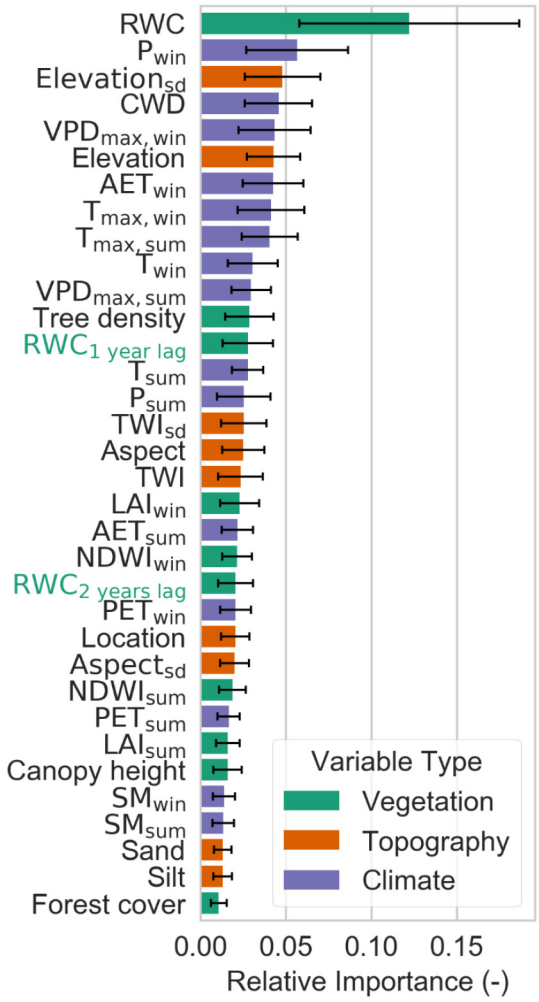

Fig. 7. Relative importance of variables in lagged model. Length of bars represent mean relative importance of variables from all 960 model runs. Error bars indicate one standard deviation on each side of mean. Abbreviations as in Table 1. The (−) symbol indicates unit-less quantities.

Cross-correlations between input variables can reduce the accuracy of relative importance rankings for machine learning. Even after excluding variables with absolute correlation coefficient > 0.5 (Fig. S6), RWC continued to be by far the most important contributor to modeling mortality as shown by the trimmed model (Fig. S7).

The lagged model showed that beyond its power for estimation, RWC holds forecasting abilities too. The addition of two extra variables, namely $RWC_{1\ year\ lag}$ and $RWC_{2\ years\ lag}$ resulted in an improved variance explained in the lagged model with $R_{test}^2 = 0.70$, and MBE = −0.001 but slightly poorer error with RMSE = 0.025. The RWC lagged by 1 year ranked 13th in the lagged model (importance = 0.03, Fig. 7), with a similar relative importance to that of current year live basal area (previously identified as a useful mortality predictor in Young et al., 2017) though less important than current year CWD (importance = 0.04). The RWC lagged by 2 years had a relative importance of 0.02.

4. Discussion

4.1. Mortality occurrence depends on RWC

A recent synthesis of drought-driven tree mortality studies found that all studied plants exhibited a decline in hydraulic conductance of at least 60% at mortality (Adams et al., 2017), though the sample size was dominated by seedlings/saplings in greenhouse settings. However, the sensitivity of xylem to cavitation – and therefore to hydraulic failure under drought – varies tremendously between species and thus across and within sites (Adams et al., 2012; Choat et al., 2012; Anderegg, 2015) making it difficult to parameterize hydraulic models at large scales (though notable counter examples exist, e.g. Tai et al., 2017). Simpler predictors of mortality have been suggested in the form of either climate metrics (Anderegg et al., 2013; Williams et al., 2013; Greenwood et al., 2017; Schwalm et al., 2017; Schwantes et al., 2017) and/or basal area (Linares et al., 2010; Young et al., 2017), but these factors do not account for spatial variability in vegetation responses to drought stress between and within species (e.g. variations in hydraulic safety margins). Our results (Fig. 3, colors in Fig. 5) show that VOD-derived RWC can integrate the actual drought stress on vegetation with variation in regional tolerance to drought and that, in the study region, it is a better indicator of tree mortality than the commonly-used CWD (Fig. 6).

Fig. 3 suggests that at stand-scale there is a threshold-like relationship between RWC and mortality occurrence. The RWC threshold for mortality was quite similar between the Northern domain (0.05, Fig. 3c) and Southern domain (0.16, Fig. 3e), despite likely dissimilarities in species composition. This shows that the RWC-mortality relationship may be relatively independent of vegetation cover and location, increasing RWC's suitability for use in empirical mortality models (Martinez-Vilalta et al., 2018). This is consistent with a relatively uniform threshold for laboratory-observed leaf RWC at turgor

loss across 89 species (Bartlett et al., 2012). However, more studies are required to confirm the expectation of a similar RWC threshold distribution across species and test whether the remaining differences between the thresholds in the two parts of the domain were due to experimental noise in the study (e.g. imperfect mortality data, uncertainties in estimating RWC from VOD) or due to underlying species-specific differences in sensitivity to VOD-derived RWC at stand scale. Most of all, further investigation is required to evaluate the imperfections in the threshold relationship (Fig. 3a). Reanalyzing the thresholds for different cause agents of mortality (e.g. Bark beetle infestation), different communities (e.g. pines, hardwood and fir) or increasing the spatial resolution of the predictor variables to decrease noise (see Section 4.2) may be some potential avenues.

It should also be noted that our VOD-based RWC definition differs from that at the physiological scale – it is normalized based on the driest and wettest naturally occurring values at 0.25° scale, not relative to complete desiccation and hydration. Furthermore, unlike in the laboratory, our VOD-based RWC definition is also sensitive to reductions in biomass over the course of the drought, since VOD depends on both biomass and relative water content per unit biomass (Momen et al., 2017). Over forested vegetation types, a biomass reduction should be reflected in reduced LAI. However, the importance ranking of both winter LAI (16th) and summer LAI (25th) in the base model is much poorer than that of RWC (1st). Moreover, the cross-correlation between mean LAI in each season and RWC (-0.07 for summer and -0.06 for winter) is also relatively low (Fig. S6). Taken together, this suggests that much of the value of RWC for estimating FAM is due to declines in the relative water content per unit biomass. To validate the hypothesis, we further checked the predictive strength of RWC per unit leaf area for FAM estimation by introducing a new variable-RWC/LAI_{sum}. This metric also does not fully account for spatio-temporal biomass changes on VOD and RWC. Nevertheless, it provides a useful first-order sensitivity analysis, as further explained in Text S1. We found that the RWC's relative importance was almost unchanged (Fig. S8), and that it was more important than RWC/LAI_{sum}. Similarly, progressive mortality over time could in theory alter the vegetation structure in a grid cell and thus its b_s. While changes in b_s may affect our calculation of RWC, we do not expect them to be a dominant driver of RWC because a change in vegetation structure significant enough to affect b_s would be expected to also affect LAI. But the poor cross-correlation between LAI and RWC suggests any b_s variations have a relatively minor influence on RWC.

While our results suggest RWC declines could be an informative indicator of drought-driven tree mortality – complementary to the more traditionally used variables for drought-driven mortality estimation – additional studies are needed to determine the validity of these findings in areas with different climatic conditions and species composition. Further research is also needed to better understand the underlying physiological mechanisms of the mortality-water content response (Guadagno et al., 2017; Martinez-Vilalta et al., 2018).

4.2. Prospects for remote sensing of RWC

The RWC can serve as an ideal indicator of mortality risk if it can be easily measured across large scales (Martinez-Vilalta et al., 2018). The estimation of RWC from remote sensing alone – as shown in this paper – is thus crucial to enable large scale studies of forest mortality. Although remote sensing assisted in overcoming challenges of scale in our case, the use of passive microwave data for estimating RWC imposed a severe constraint on spatial resolution. Because of the non-linear relationship between RWC and FAM (Fig. 3), the high intra-pixel heterogeneity in RWC grid cells at 0.25° likely reduced the accuracy of the base model (Fig. 5). The coarse spatial resolution also resulted in a relatively small number of high FAM-pixels (only 10% of the pixels have FAM ≥ 0.05), further degrading model accuracy. Due to very few pixel-years with high FAM, the model was unable to train optimally in the corresponding regions of the feature space resulting in consistent underestimation of mortality. Lastly, and perhaps most importantly, the utility of FAM predictions is partially limited by its coarse resolution. Alternate remote sensing observations sensitive to RWC available at higher spatial resolution are therefore needed.

Previous studies have used multispectral and hyperspectral remote sensing in combination with machine learning (including random forests) to classify high-resolution mortality occurrence depending on observed properties of the vegetation itself (Byer and Jin, 2017; Tane et al., 2018). Such studies have primarily focused on mapping past mortality rather than modeling present or future mortality using a variable with a clear physiological basis as in our study (cf. Martinez-Vilalta et al., 2018). Although NDWI is frequently used to detect drought stress (Gu et al., 2007) and can thus help in modeling processes leading to mortality, its low importance ranking in the random forest model suggests that it is not as indicative of drought stress as microwave-based RWC. This may be due to the sparse temporal resolution of MODIS (8 days) leading to only a handful of observations in the summer and winter seasons of each year or more fundamentally, due to limitations of the shortwave infrared observations themselves in capturing whole plant water status. Additionally, hyperspectral observations have been used previously to retrieve water content over short timescales for small domains (e.g. Serrano et al., 2000; Asner et al., 2016; Romero Ramirez et al., 2018) which can be used to model mortality (Brodrick and Asner, 2017). Asner et al. (2016) used hyperspectral observations from the Carnegie Airborne Observatory (CAO) at high spatial resolution across the Sierra Nevada region for the years 2015 and 2016. However, airborne observation platforms are cost-prohibitive across longer timescales and larger spatial domains. For the CAO data, this resulted in a need to use additional modeling to extend the observational record for mortality studies (Brodrick and Asner, 2017). Little is known about the efficacy of these methods over longer time periods, since they are not directly driven by observations of mortality. Because there are currently no publicly available spaceborne hyperspectral instruments, the availability of hyperspectral data is limited to areas where specific field campaigns were conducted, and rarely allows for multiyear records (unless alternative methods are used to predict longer records based on observed years, as in Brodrick and Asner, 2017). Hyperspectral earth-observing satellites are likely to be launched in the next decade (Lee et al., 2015), and this approach holds strong potential for the study of forest mortality in the future.

Alternatively, Synthetic Aperture Radar (SAR) may prove useful for modeling of drought-driven tree mortality. SAR observations are made by several currently operational satellites (Steele-Dunne et al., 2017). Analogous to their passive radiometry counterpart operating at similar electromagnetic frequencies (e.g. the AMSR-E data used here), SAR measurements are sensitive to VWC. However, the VWC retrieval from SAR measurements is highly dependent on vegetation canopy characteristics (Ulaby et al., 1988; Ulaby and Long, 2014) and generalized, scalable algorithms do not currently exist for VWC retrieval from SAR observations. While some simplified scattering models exist (e.g. Saatchi et al., 2007), they are difficult to parametrize across large scales. Recent successes in improved radar retrieval of soil moisture without prior vegetation geometry parameters (Bruscantini et al., 2015) suggest that VWC retrievals from SAR may be possible. Because SAR observations are several orders of magnitude higher resolution than radiometric observations (3–4 orders of magnitude smaller pixel area), development of such algorithms could dramatically improve the potential uses of RWC for mortality modeling and forecasting.

4.3. RWC can assist in forecasting mortality

While RWC can be used to model FAM, it is unclear to what degree this relationship is because RWC is sensitive to recent mortality (dead trees are dry and may have reduced biomass) or because it is an indicator of water stress that is a pre-cursor to mortality. Compared to current year variables, the RWC showed a moderate ability to forecast

mortality at yearly timescales, with RWC lagged by 1 year (rank 13th) found to be about 38% less useful than CWD of the current year (rank 4th) in the lagged model (Fig. 7). With RWC lagged by two years, the contribution to mortality predictions almost disappears. It is hypothetically possible that the moderately good rank of $RWC_{1\ year\ lag}$ is solely due to a cross-correlation between previous years' mortality and current mortality, and an influence of previous years' mortality on current RWC (e.g. RWC detecting past mortality). However, because there is only a weak correlation between incremental FAM and cumulative FAM ($R^2 = 0.28$ for pixels with FAM ≥ 0.1, Fig. S4), this is unlikely, but more research is required to disentangle the effect of cross-correlation from the true predictive capability of RWC. Further determination of the degree to which our results are driven by mortality detection rather than forecasting is limited by the coarse temporal resolution of the mortality data (1 year), with flights spread out over several months. Nevertheless, when taken together, the results of the lagged model and the fact that RWC is a measure of the underlying water status of the vegetation suggest that it may be possible for RWC observations to eventually provide early warning signals of future mortality risk, as also suggested by Brodrick and Asner (2017).

5. Conclusion

We presented a novel method to estimate ecosystem-scale relative water content (RWC) solely using satellite-based vegetation optical depth (VOD). The results of the study provide landscape-scale support to confirm previous laboratory-based studies suggesting RWC is a predictor of mortality (e.g., Kursar et al., 2009). Comparison of RWC with fractional area of mortality (FAM) revealed that RWC has a stronger threshold relationship with FAM than the widely used climatic water deficit (CWD). Furthermore, the threshold for RWC was found to be relatively insensitive to local climatic and vegetation characteristics. Separately, when compared against all possible climatic, topographic, and vegetation-related predictors of tree mortality, RWC was the best predictor (importance = 0.11/1.00) in a random forests machine learning model with satisfactory performance ($R_{test}^2 = 0.66$). The RWC significantly complemented alternate variables in estimation of drought-driven tree mortality. The relationship between RWC and FAM – either through breakpoint threshold regression or machine learning based predictions – remains noisy, although this may be improved in part with higher-resolution RWC data. While the California forests cover a wide variety of species with different drought response strategies, the utility of RWC should be tested in additional climates to gain more confidence in its prediction robustness. Nevertheless, because it is both directly related to vegetation water stress and easily observable remotely, RWC remains promising for mortality studies at a variety of spatial scales.

Acknowledgements

This research was supported by the UPS Endowment Fund at Stanford and NASA Terrestrial Ecology (award 80NSSC18K0715) through New (Early Career) Investigator program to AGK. JMV was partially supported by Spanish grant CGL2013-46808-R and by an ICREA Academia award. W.R.L.A. acknowledges funding from the University of Utah Global Change and Sustainability Center, NSF Grant 1714972, and the USDA National Institute of Food and Agriculture, Agricultural and Food Research Initiative Competitive Programme, Ecosystem Services and Agro-ecosystem Management, grant no. 2018-67019-27850. AS was partially supported by the National Science Foundation (BCS 1461576).

Data accessibility

The code used to retrieve, re-grid data sets from public sources, and the code used to perform statistical analyses are available in GitHub Repository: https://github.com/kkraoj/tree_mortality_from_vod

Appendix A. Supplementary data

Supplementary data to this article can be found online at https://doi.org/10.1016/j.rse.2019.03.026.

References

Adams, H.D., Luce, C.H., Breshears, D.D., Allen, C.D., Weiler, M., Hale, V.C., et al., 2012. Ecohydrological consequences of drought- and infestation-triggered tree die-off: insights and hypotheses. Ecohydrology 5, 145–159.
Adams, H.D., Williams, A.P., Xu, C., Rauscher, S.A., Jiang, X., McDowell, N.G., 2013. Empirical and process-based approaches to climate-induced forest mortality models. Front. Plant Sci. 4, 438.
Adams, H.D., Zeppel, M.J.B., Anderegg, W.R.L., Hartmann, H., Landhäusser, S.M., Tissue, D.T., et al., 2017. A multi-species synthesis of physiological mechanisms in drought-induced tree mortality. Nat. Ecol. Evol. 1, 1285–1291.
Allen, C.D., Breshears, D.D., McDowell, N.G., 2015. On underestimation of global vulnerability to tree mortality and forest die-off from hotter drought in the Anthropocene. Ecosphere 6, 1–55.
Anderegg, L.D.L., Anderegg, W.R.L., Abatzoglou, J., Hausladen, A.M., Berry, J.A., 2013. Drought characteristics' role in widespread aspen forest mortality across Colorado, USA. Glob. Chang. Biol. 19, 1526–1537.
Anderegg, W.R.L., 2015. Spatial and temporal variation in plant hydraulic traits and their relevance for climate change impacts on vegetation. New Phytol. 205, 1008–1014.
Anderegg, W.R.L., Flint, A., Huang, C., Flint, L., Berry, J.A., Davis, F.W., et al., 2015a. Tree mortality predicted from drought-induced vascular damage. Nat. Geosci. 8, 367–371.
Anderegg, W.R.L., Hicke, J.A., Fisher, R.A., Allen, C.D., Aukema, J., Bentz, B., et al., 2015b. Tree mortality from drought, insects, and their interactions in a changing climate. New Phytol. 208, 674–683.
Anderegg, W.R.L., Klein, T., Bartlett, M., Sack, L., Pellegrini, A.F.A., Choat, B., et al., 2016. Meta-analysis reveals that hydraulic traits explain cross-species patterns of drought-induced tree mortality across the globe. Proc. Natl. Acad. Sci. 113, 5024–5029.
Arino, O., Perez, J.R., Kalogirou, V., Defourny, P., Achard, F., 2010. Globcover 2009. In: ESA Living Planet Symp, pp. 1–3.
Asner, G.P., Brodrick, P.G., Anderson, C.B., Vaughn, N., Knapp, D.E., Martin, R.E., 2016. Progressive forest canopy water loss during the 2012–2015 California drought. Proc. Natl. Acad. Sci. 113, E249–E255.
Attema, E.P.W., Ulaby, F.T., 1978. Vegetation modeled as a water cloud. Radio Sci. 13, 357–364.
Bart, R.R., Tague, C.L., Moritz, M.A., 2016. Effect of tree-to-shrub type conversion in lower montane forests of the Sierra Nevada (USA) on streamflow. PLoS One 11, 1–19.
Bartlett, M.K., Klein, T., Jansen, S., Choat, B., Sack, L., 2016. The correlations and sequence of plant stomatal, hydraulic, and wilting responses to drought. Proc. Natl. Acad. Sci. 113, 13098–13103.
Bartlett, M.K., Scoffoni, C., Sack, L., 2012. The determinants of leaf turgor loss point and prediction of drought tolerance of species and biomes: a global meta-analysis. Ecol. Lett. 15, 393–405.
Beven, K.J., Kirkby, M.J., Kirkby, A.J., 1979. A physically based, variable contributing area model of basin hydrology/Un modèle à base physique de zone d'appel variable de l'hydrologie du bassin versant. Hydrol. Sci. J. 24, 43–69.
Bigler, C., Gavin, D.G., Gunning, C., Veblen, T.T., 2007. Drought induces lagged tree mortality in a subalpine forest in the Rocky Mountains. Oikos 116, 1983–1994.
Bigler, C., Veblen, T.T., 2011. Changes in litter and dead wood loads following tree death beneath subalpine conifer species in northern Colorado. Can. J. For. Res. 41, 331–340.
Bréda, N., Huc, R., Granier, A., Dreyer, E., 2006. Temperate forest trees and stands under severe drought: a review of ecophysiological responses, adaptation processes and long-term consequences. Ann. For. Sci. 63, 625–644.
Breiman, L., 2001. Random forests. Mach. Learn. 45, 5–32.
Brodrick, P.G., Asner, G.P., 2017. Remotely sensed predictors of conifer tree mortality during severe drought. Environ. Res. Lett. 12, 115013.
Bruscantini, C.A., Konings, A.G., Narvekar, P.S., McColl, K.A., Entekhabi, D., Grings, F.M., et al., 2015. L-band radar soil moisture retrieval without ancillary information. IEEE J. Sel. Top. Appl. Earth Obs. Remote Sens. 8, 5526–5540.
Byer, S., Jin, Y., 2017. Detecting drought-induced tree mortality in Sierra Nevada forests with time series of satellite data. Remote Sens. 9, 929.
Chaparro, D., Vayreda, J., Vall-Llossera, M., Banque, M., Piles, M., Camps, A., et al., 2017. The role of climatic anomalies and soil moisture in the decline of drought-prone forests. IEEE J. Sel. Top. Appl. Earth Obs. Remote Sens. 10, 503–514.
Choat, B., Jansen, S., Brodribb, T.J., Cochard, H., Delzon, S., Bhaskar, R., et al., 2012. Global convergence in the vulnerability of forests to drought. Nature 491, 752–755.
De Toledo, J.J., Magnusson, W.E., Castilho, C.V., Nascimento, H.E.M., 2011. How much variation in tree mortality is predicted by soil and topography in Central Amazonia? For. Ecol. Manag. 262, 331–338.
Du, J., Kimball, J.S., Jones, L.A., Kim, Y., Glassy, J., Watts, J.D., 2017. A global satellite environmental data record derived from AMSR-E and AMSR2 microwave Earth observations. Earth Syst. Sci. Data 9, 791–808.
Du, J., Kimball, J.S., Jones, L.A., Member, S., 2016. Passive microwave remote sensing of soil moisture based on dynamic vegetation scattering properties for AMSR-E. IEEE

Trans. Geosci. Remote Sens. 1–12.
Du, J., Kimball, J.S., Shi, J., Jones, L.A., Wu, S., Sun, R., et al., 2014. Inter-calibration of satellite passive microwave land observations from AMSR-E and AMSR2 using overlapping FY3B-MWRI sensor measurements. Remote Sens. 6, 8594–8616.
Fassnacht, F.E., Latifi, H., Ghosh, A., Joshi, P.K., Koch, B., 2014. Assessing the potential of hyperspectral imagery to map bark beetle-induced tree mortality. Remote Sens. Environ. 140, 533–548.
Fernandez-Moran, R., Al-Yaari, A., Mialon, A., Mahmoodi, A., Al Bitar, A., De Lannoy, G., et al., 2017. SMOS-IC: an alternative SMOS soil moisture and vegetation optical depth product. Remote Sens. 9, 1–21.
Gao, B.C., 1996. NDWI - a normalized difference water index for remote sensing of vegetation liquid water from space. Remote Sens. Environ. 58, 257–266.
Greenwood, S., Ruiz-Benito, P., Martínez-Vilalta, J., Lloret, F., Kitzberger, T., Allen, C.D., et al., 2017. Tree mortality across biomes is promoted by drought intensity, lower wood density and higher specific leaf area. Ecol. Lett. 20, 539–553.
Gu, Y., Brown, J.F., Verdin, J.P., Wardlow, B., 2007. A five-year analysis of MODIS NDVI and NDWI for grassland drought assessment over the central Great Plains of the United States. Geophys. Res. Lett. 34, 1–6.
Guadagno, C.R., Ewers, B.E., Speckman, H.N., Aston, T.L., Huhn, B.J., DeVore, S.B., et al., 2017. Dead or alive? Using membrane failure and chlorophyll fluorescence to predict mortality from drought. Plant Physiol. 175, 00581 (2016).
Hanson, P.J., Weltzin, J.F., 2000. Drought disturbance from climate change: response of United States forests. Sci. Total Environ. 262, 205–220.
Harrison, P.A., Berry, P.M., Simpson, G., Haslett, J.R., Blicharska, M., Bucur, M., et al., 2014. Linkages between biodiversity attributes and ecosystem services: a systematic review. Ecosyst. Serv. 9, 191–203.
Hartmann, H., Moura, C.F., Anderegg, W.R.L., Ruehr, N.K., Salmon, Y., Allen, C.D., et al., 2018. Research frontiers for improving our understanding of drought-induced tree and forest mortality. New Phytol. 218, 15–28.
Hicke, J.A., Meddens, A.J.H., Kolden, C.A., 2016. Recent tree mortality in the Western United States from bark beetles and forest fires. For. Sci. 62, 141–153.
Hogg, E. (Ted), Brandt, J.P. & Kochtubajda, B. (2005). Factors affecting interannual variation in growth of western Canadian aspen forests during 1951–2000. Can. J. For. Res., 35, 610–622.
Jackson, T.J., O'Neill, P.E., 1990. Attenuation of Soil Microwave Emissivity by Corn And Soybeans at 1.4 and 5 GHz. IEEE, pp. 1165–1168.
Jackson, T.J., Schmugge, T.J., 1991. Vegetation effects on the microwave emission of soils. Remote Sens. Environ. 36, 203–212.
Jones, E., Oliphant, T., Peterson, P., et al., 2011a. SciPy: Open Source Scientific Tools for Python.
Jones, M.O., Jones, L.A., Kimball, J.S., McDonald, K.C., 2011b. Satellite passive microwave remote sensing for monitoring global land surface phenology. Remote Sens. Environ. 115, 1102–1114.
Kaiser, K.E., McGlynn, B.L., Emanuel, R.E., 2013. Ecohydrology of an outbreak: mountain pine beetle impacts trees in drier landscape positions first. Ecohydrology 6, 444–454.
Konings, A.G., McColl, K.A., Piles, M., Entekhabi, D., 2015. How many parameters can be maximally estimated from a set of measurements? IEEE Geosci. Remote Sens. Lett. 12, 1081–1085.
Konings, A.G., Piles, M., Das, N., Entekhabi, D., 2017. L-band vegetation optical depth and effective scattering albedo estimation from SMAP. Remote Sens. Environ. 198, 460–470.
Konings, A.G., Piles, M., Rötzer, K., McColl, K.A., Chan, S.K., Entekhabi, D., 2016. Vegetation optical depth and scattering albedo retrieval using time series of dual-polarized L-band radiometer observations. Remote Sens. Environ. 172, 178–189.
Kursar, T.A., Engelbrecht, B.M.J., Burke, A., Tyree, M.T., El Omari, B., Giraldo, J.P., 2009. Tolerance to low leaf water status of tropical tree seedlings is related to drought performance and distribution. Funct. Ecol. 23, 93–102.
Land Ecology Modeling & Analysis Group, 2015. GNN structure (species-size) maps. Available at. https://lemma.forestry.oregonstate.edu/data/structure-maps, Accessed date: 8 May 2018.
Lee, C.M., Cable, M.L., Hook, S.J., Green, R.O., Ustin, S.L., Mandl, D.J., et al., 2015. An introduction to the NASA hyperspectral InfraRed imager (HyspIRI) mission and preparatory activities. Remote Sens. Environ. 167, 6–19.
Li, Y., Guan, K., Gentine, P., Konings, A.G., Meinzer, F.C., Kimball, J.S., et al., 2017. Estimating global ecosystem isohydry/anisohydry using active and passive microwave satellite data. J. Geophys. Res. Biogeosci. 122, 3306–3321.
Linares, J.C., Camarero, J.J., Carreira, J.A., 2010. Competition modulates the adaptation capacity of forests to climatic stress: insights from recent growth decline and death in relict stands of the Mediterranean fir *Abies pinsapo*. J. Ecol. 98, 592–603.
Liu, S., Wei, Y., Post, W.M., Cook, R.B., Schaefer, K., Thorton, M.M., 2014. NACP MsTMIP: Unified North American Soil Map.
Malone, T., Liang, J., Packee, E.C., 2009. Cooperative Alaska Forest Inventory.
Martinez-Vilalta, J., Anderegg, W.R.L., Sapes, G., Sala, A., 2018. Greater focus on water pools may improve our ability to understand and anticipate drought-induced mortality in plants. New Phytol. https://doi.org/10.1111/nph.15644.
Martínez-Vilalta, J., Piñol, J., Beven, K., 2002. A hydraulic model to predict drought-induced mortality in woody plants: an application to climate change in the Mediterranean. Ecol. Model. 155, 127–147.
McDowell, N., Pockman, W.T., Allen, C.D., Breshears, D.D., Cobb, N., Kolb, T., et al., 2008. Mechanisms of plant survival and mortality during drought: why do some plants survive while others succumb to drought? New Phytol. 178, 719–739.
Mcdowell, N.G., Fisher, R.A., Xu, C., Domec, J.C., Hölttä, T., Mackay, D.S., et al., 2013. Evaluating theories of drought-induced vegetation mortality using a multimodel-experiment framework. New Phytol. 200, 304–321.
McFarlane, B.L., Witson, D.O.T., 2008. Perceptions of ecological risk associated with mountain pine beetle (Dendroctonus ponderosae) infestations in Banff and Kootenay National Parks of Canada. Risk Anal. 28, 203–212.
McIntyre, P.J., Thorne, J.H., Dolanc, C.R., Flint, A.L., Flint, L.E., Kelly, M., et al., 2015. Twentieth-century shifts in forest structure in California: denser forests, smaller trees, and increased dominance of oaks. Proc. Natl. Acad. Sci. 112, 1458–1463.
Meddens, A.J.H., Hicke, J.A., Vierling, L.A., Hudak, A.T., 2013. Evaluating methods to detect bark beetle-caused tree mortality using single-date and multi-date Landsat imagery. Remote Sens. Environ. 132, 49–58.
Meigs, G.W., Kennedy, R.E., Cohen, W.B., 2011. A Landsat time series approach to characterize bark beetle and defoliator impacts on tree mortality and surface fuels in conifer forests. Remote Sens. Environ. 115, 3707–3718.
Momen, M., Wood, J.D., Novick, K.A., Pangle, R., Pockman, W.T., McDowell, N.G., et al., 2017. Interacting effects of leaf water potential and biomass on vegetation optical depth. J. Geophys. Res. Biogeosci. 122, 3031–3046.
Oyler, J.W., Ballantyne, A., Jencso, K., Sweet, M., Running, S.W., 2015. Creating a topoclimatic daily air temperature dataset for the conterminous United States using homogenized station data and remotely sensed land skin temperature. Int. J. Climatol. 35, 2258–2279.
PRISM Climate Group Oregon State University, 2016. PRISM Climate Data. Available at: http://prism.oregonstate.edu/, Accessed date: 1 March 2018.
R Core Team, 2016. R: A Language and Environment for Statistical Computing.
Reichle, R.H., Koster, R.D., 2004. Bias reduction in short records of satellite soil moisture. Geophys. Res. Lett. 31, 2–5.
Romero Ramirez, F.J., Navarro-Cerrillo, R.M., Varo-Martínez, M.Á., Quero, J.L., Doerr, S., Hernández-Clemente, R., 2018. Determination of forest fuels characteristics in mortality-affected Pinus forests using integrated hyperspectral and ALS data. Int. J. Appl. Earth Obs. Geoinf. 68, 157–167.
Saatchi, S., Halligan, K., Despain, D.G., Crabtree, R.L., 2007. Estimation of forest fuel load from radar remote sensing. IEEE Trans. Geosci. Remote Sens. 45, 1726–1740.
Sala, A., Piper, F., Hoch, G., 2010. Physiological mechanisms of drought-induced tree mortality are far from being resolved. New Phytol. 186, 274–281.
Schaaf, C., Wang, Z., 2015. MCD43A4 V006|LP DAAC: NASA land data products and services. Available at: https://lpdaac.usgs.gov/dataset_discovery/modis/modis_products_table/mcd43a4_v006, Accessed date: 29 January 2019.
Schwalm, C.R., Anderegg, W.R.L., Michalak, A.M., Fisher, J.B., Biondi, F., Koch, G., et al., 2017. Global patterns of drought recovery. Nature 548, 202–205.
Schwantes, A.M., Swenson, J.J., González-Roglich, M., Johnson, D.M., Domec, J.C., Jackson, R.B., 2017. Measuring canopy loss and climatic thresholds from an extreme drought along a fivefold precipitation gradient across Texas. Glob. Chang. Biol. 23, 5120–5135.
Serrano, L., Ustin, S.L., Roberts, D.A., Gamon, J.A., Peñuelas, J., 2000. Deriving water content of chaparral vegetation from AVIRIS data. Remote Sens. Environ. 74, 570–581.
Simard, M., Pinto, N., Fisher, J.B., Baccini, A., 2011. Mapping forest canopy height globally with spaceborne lidar. J. Geophys. Res. Biogeosci. 116, 1–12.
Steele-Dunne, S.C., McNairn, H., Monsivais-Huertero, A., Judge, J., Liu, P.W., Papathanassiou, K., 2017. Radar remote sensing of agricultural canopies: a review. IEEE J. Sel. Top. Appl. Earth Obs. Remote Sens. 10, 2249–2273.
Stephens, S.L., Collins, B.M., Fettig, C.J., Finney, M.A., Hoffman, C.M., Knapp, E.E., et al., 2018. Drought, tree mortality, and wildfire in forests adapted to frequent fire. Bioscience 68, 77–88.
Stephenson, N., 1998. Actual evapotranspiration and deficit: biologically meaningful correlates of vegetation distribution across spatial scales. J. Biogeogr. 25, 855–870.
Swain, D.L., Tsiang, M., Haugen, M., Singh, D., Charland, A., Rajaratnam, B., et al., 2014. The extraordinary California drought of 2013/2014: character, context, and the role of climate change. Bull. Amer. Meteor. Soc. 95, S3–S7.
Swatantran, A., Dubayah, R., Roberts, D., Hofton, M., Blair, J.B., 2011. Mapping biomass and stress in the Sierra Nevada using lidar and hyperspectral data fusion. Remote Sens. Environ. 115, 2917–2930.
Tai, X., Mackay, D.S., Anderegg, W.R.L., Sperry, J.S., Brooks, P.D., 2017. Plant hydraulics improves and topography mediates prediction of aspen mortality in southwestern USA. New Phytol. 213, 113–127.
Tane, Z., Roberts, D., Koltunov, A., Sweeney, S., Ramirez, C., 2018. A framework for detecting conifer mortality across an ecoregion using high spatial resolution space-borne imaging spectroscopy. Remote Sens. Environ. 209, 195–210.
Tian, F., Brandt, M., Liu, Y.Y., Verger, A., Tagesson, T., Diouf, A.A., et al., 2016. Remote sensing of vegetation dynamics in drylands: evaluating vegetation optical depth (VOD) using AVHRR NDVI and in situ green biomass data over West African Sahel. Remote Sens. Environ. 177, 265–276.
Ulaby, F.T., Long, D.G., 2014. Microwave Radar and Radiometric Remote Sensing. University of Michigan Press, Ann Arbor.
Ulaby, F.T., McDonald, K., Sarabandi, K., Dobson, M.C., 1988. Michigan microwave canopy scattering models (MIMICS). Int. Geosci. Remote Sens. Symp. "Remote Sens. Mov. Towar. 21st Century" 2, 1009.
United States Department of Agriculture Forest Service, 2017. Aerial detection and monitoring program. Available at: https://www.fs.usda.gov/detail/r5/forest-grasslandhealth/?cid=fsbdev3_046696, Accessed date: 1 March 2018.
USDA, 2016. News Release New Aerial Survey Identifies More than 100 Million Dead Trees in California.
USGS, 2000. HYDRO1k | the Long term archive. Available at: https://lta.cr.usgs.gov/HYDRO1KReadMe, Accessed date: 13 November 2018.
USGS, 2011a. National Elevation Dataset. Available at: https://nationalmap.gov/elevation.html, Accessed date: 14 August 2016.
USGS, 2011b. National GAP Analysis Project (GAP). Available at. https://gapanalysis.usgs.gov/data/web-services/, Accessed date: 14 August 2016.
Van De Griend, A.A., Wigneron, J.P., 2004. The b-factor as a function of frequency and canopy type at H-polarization. IEEE Trans. Geosci. Remote Sens. 42, 786–794.

Van Mantgem, P.J., Stephenson, N.L., 2007. Apparent climatically induced increase of tree mortality rates in a temperate forest. Ecol. Lett. 10, 909–916.
Verbesselt, J., Robinson, A., Stone, C., Culvenor, D., 2009. Forecasting tree mortality using change metrics derived from MODIS satellite data. For. Ecol. Manag. 258, 1166–1173.
Williams, A.P., Allen, C.D., Macalady, A.K., Griffin, D., Woodhouse, C.A., Meko, D.M., et al., 2013. Temperature as a potent driver of regional forest drought stress and tree mortality. Nat. Clim. Chang. 3, 292–297.
Willmott, C.J., Rowe, C.M., Mintz, Y., 1985. Climatology of the terrestrial seasonal water cycle. J. Climatol. 5, 589–606.
Worrall, J.J., Egeland, L., Eager, T., Mask, R.A., Johnson, E.W., Kemp, P.A., et al., 2008. Rapid mortality of Populus tremuloides in southwestern Colorado, USA. For. Ecol. Manag. 255, 686–696.
Wright, M.N., Ziegler, A., 2015. Ranger: a fast implementation of random forests for high dimensional data in C++ and R. J. Stat. Softw. 77, 1–17.
Xia, Y., Mitchell, K., Ek, M., Sheffield, J., Cosgrove, B., Wood, E., et al., 2012. Continental-scale water and energy flux analysis and validation for the north American land data assimilation system project phase 2 (NLDAS-2): 1. Intercomparison and application of model products. J. Geophys. Res. Atmos. 117 (n/a-n/a).
Xiong, Y., D'Atri, J.J., Fu, S., Xia, H., Seastedt, T.R., 2011. Rapid soil organic matter loss from forest dieback in a subalpine coniferous ecosystem. Soil Biol. Biochem. 43, 2450–2456.
Young, D.J.N., Stevens, J.T., Earles, J.M., Moore, J., Ellis, A., Jirka, A.L., et al., 2017. Long-term climate and competition explain forest mortality patterns under extreme drought. Ecol. Lett. 20, 78–86.
Yuan, H., Dai, Y., Xiao, Z., Ji, D., Shangguan, W., 2011. Reprocessing the MODIS leaf area index products for land surface and climate modelling. Remote Sens. Environ. 115, 1171–1187.
Zarco-Tejada, P.J., Miller, J.R., Mohammed, G.H., Noland, T.L., Sampson, P.H., 2002. Vegetation stress detection through chlorophyll + estimation and fluorescence effects on hyperspectral imagery. J. Environ. Qual. 31, 1433.